J. Fluid Mech. (1990), *vol.* 214, *pp.* 469–487
Printed in Great Britain

Study on the flow structure around a flat plate in a stagnation flow field

By YONG KWEON SUH[1] AND CHING SHI LIU[2]

[1] Department of Mechanical Engineering, Dong-A University, Korea

[2] Department of Mechanical and Aerospace Engineering, State University of New York at Buffalo, Amherst, NY 14260, USA

(Received 22 September 1988 and in revised form 23 October 1989)

Numerical solutions have been obtained for steady viscous flow past a finite flat plate attached normally to an infinite wall at Reynolds numbers Re up to 2800. Separately, Levi-Civita's method has been used to obtain the flow solution based on the free-streamline theory. Apart from the case of uniform flow past an isolated obstacle, the present flow problem appeared to exhibit the validity of the free-streamline model for the global structure of the flow field. The position of the separation point could be predicted by two terms of the asymptotic solution based on the Sychev–Smith model within 0.6% error for the range $100 \leqslant Re \leqslant 2800$.

1. Introduction

The nature of the boundary-layer separation at high Reynolds numbers is a problem of the most fundamental interest in fluid mechanics. It concerns not only the development of the boundary layer upstream but also the structures of the wake downstream and the potential zone elsewhere. For a bluff body submerged in a uniform stream, for instance, the shape of the wake is generally unknown *a priori*, and so the position of the separation point as well as the characteristics of the boundary layer upstream must be determined as a part of the problem. The boundary layer, the wake and the potential zone thus interact with each other rendering the analysis difficult and complicated.

In each of the variety of wake models which have been proposed by many theoreticians, at least one of the three regions was ignored to simplify the problem. Kirchhoff (1869) ignored the boundary layer, and assumed that the fluid within the eddy of the wake is totally motionless and the particle velocity on the free streamline is equal to that of the uniform flow far upstream of the body. The free-streamline theory later developed by a number of investigators (see e.g. Wu 1972) results in a finite drag coefficient and an open wake. Although the drag may or may not be finite (see Batchelor 1956*b*), at asymptotically large Reynolds numbers an open wake is not desirable since it does not represent the true picture of nature at large but finite Reynolds numbers. A physically and mathematically detailed argument concerning this matter is given in Batchelor (1956*b*). Batchelor's proposal (1956*a*) then appeared in a quite different light. He also ignored the boundary layer, but assumed that the wake is closed and proved that within the closed wake, vorticity is constant. Thus Batchelor's model is composed of two regions. One of the important properties of this model is the zero drag coefficient.

The above two basic models are simple but incomplete since the viscous effects are

ignored and as a result there is at least one unknown constant in the calculation. Smith's (1985, 1986) model includes finite drag and closed wake. (The corresponding basic-flow model was studied earlier by Sadovskii 1971 and its relevance to circular-cylinder-flow was implied numerically by Fornberg 1986.) Smith's model has two main regions; a large-scale flow of $O(Re)$ and a body-scale flow of $O(1)$. The former comprises symmetric eddies, each with a uniform level of vorticity, and the potential zone elsewhere. Along the dividing lines are viscous shear layers. In the body-scale flow, the two main regions are the open wake and the potential zone outside. There is a boundary layer adjacent to the body and a shear layer between the two inviscid regions. In the region near the separation point, triple-deck iteration must be applied. The open wake and the shear layer are matched with the corresponding small regions in the large-scale flow. Thus Smith's model appears to be more complete than any previous one. But it still requires further resolution. For instance, Peregrine (1985) presented a detailed account of the flow mechanism near the eddy-closure region, and he suggested an exact solution of the Navier–Stokes equations for that region, which Smith did not consider fully. In addition, computation of Smith's model for the whole flow field is formidable.

We should seek a problem not complicated in modelling but still preserving the fundamental properties of separated flow from a smooth surface. The complexity in Smith's model primarily rests on the fact that the large eddies and the potential region must 'interact' in a self-consistent manner. The free-streamline model on the other hand is free of interaction, and moreover it is strongly recommended as the right local model for self-consistent boundary-layer separation (see Sychev 1972 and Smith 1977). The objection to Kirchhoff's model is the wake's openness; the free streamline reattaching downstream is also possible, as studied by Southwell & Vaisey (1946), but it persistently contains an infinite radius of curvature at the breakaway point and is rejected on triple-deck grounds.

We consider in this study flow over a finite flat plate attached normally to an infinite wall as shown in figure 1. The problem is two-dimensional, and the whole flow field is assumed to be steady, incompressible and laminar. This geometry gives rise to stagnation point flow. Owing to the corner singularity, the boundary-layer flow will separate ahead the corner. But intuitively we can conjecture that the size of the eddy remains at most of the order of the plate length because of the strongly favourable pressure gradient downstream of the wall. Thus the wake will not be open and its size will be finite even at infinite Reynolds numbers. Furthermore the boundaries are geometrically very simple, which makes it easier to find the inviscid-flow solution. In summary, the present model problem has simple boundaries but retains a closed and finite wake, which motivated the authors to study it.

Chernyshenko (1984) considered the same problem and obtained the inviscid solutions for the potential zone and the wake. One of the key assumptions in his study is that the wake is composed of one eddy with a constant vorticity. The validity of the constant vorticity is impossible (Batchelor's theorem) but not the single-eddy assumption. Leal (1973) also studied a very similar problem. The only difference lies in that the infinite wall of the present problem is replaced in his by a symmetry line along which the vorticity is zero. He predicted that the ultimate separation position at infinite Reynolds number would be a finite distance downstream of the leading edge. It should be mentioned in addition that when the blowing velocity is $O(1)$ the plate-injection problem has a very similar nature as far as the separation region is concerned. For instance Smith & Stewartson (1973) predicted that the separation point would move upstream to the leading edge

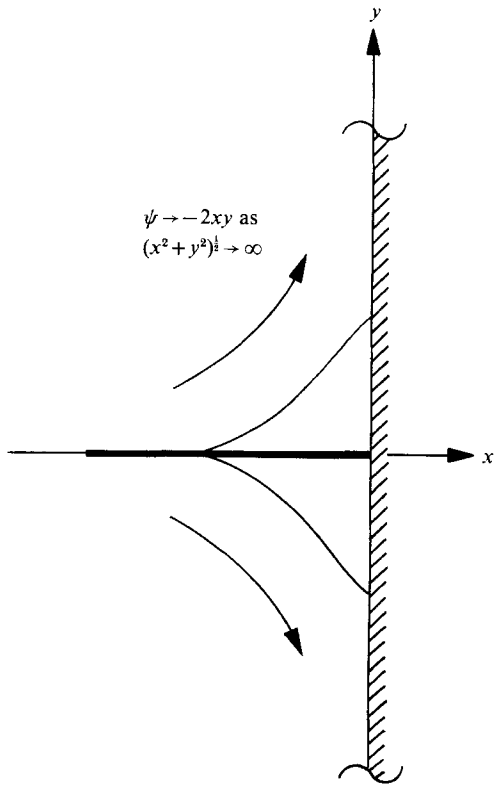

FIGURE 1. A finite flat plate attached normally to an infinite wall subject to stagnation-point flow.

asymptotically at large Reynolds numbers. At the stage of final corrections to this paper, the authors were introduced to the work of Moore, Saffman & Tanveer (1988), who obtained inviscid solutions for this problem with the single-eddy model. They added to the work of Chernyshenko (1984) by allowing for a range of eddy vorticities. They also obtained a solution for zero vorticity which we independently derive in a different form in §3.1.

The important questions to be pursued in this study are: first, what will be the structure of the recirculating flow; second, what will be the inviscid solution valid in the potential zone; and finally, how may triple-deck theory be applied to predict the separation position? The first and second questions are associated with Chernyshenko's study and the third with Leal's and that of Smith & Stewartson (1973).

2. Formulation of the problem

We consider a finite flat plate attached normally to an infinite wall as shown in figure 1. The problem is two-dimensional and the whole flow field is assumed to be steady, incompressible and laminar. The length of the plate, without loss of generality, can be taken 1, and the stream function in the potential region far from the corner can be set asymptotically as

$$\psi \sim -2xy. \tag{1}$$

The Navier–Stokes equations are then formulated in terms of ψ:

$$\nabla^4\psi - Re\frac{\partial(\psi, \nabla^2\psi)}{\partial(y, x)} = 0, \tag{2}$$

where $\nabla^2 = (\partial^2/\partial x^2) + (\partial^2/\partial y^2)$ and the Reynolds number Re is $1/\nu$. Symmetry is assumed and consideration of the quarter-plane $y \geqslant 0$, $x \leqslant 0$ is sufficient. The boundary conditions are

$$\psi(x, 0) = \psi(0, y) = 0, \tag{3a}$$

$$\frac{\partial\psi}{\partial y}(x, 0) = 0 \quad \text{for} \quad -1 \leqslant x \leqslant 0, \tag{3b}$$

$$\frac{\partial\psi}{\partial x}(0, y) = 0 \quad \text{for} \quad 0 \leqslant y, \tag{3c}$$

$$\frac{\partial^2\psi}{\partial y^2}(x, 0) = 0 \quad \text{for} \quad x < -1 \tag{3d}$$

and

$$\psi \to -2xy \quad \text{as} \quad (x^2 + y^2)^{\frac{1}{2}} \to \infty. \tag{3e}$$

The full equation (2) will be solved numerically by the method shown in §4.

Our concern in this study is the structure of the flow field at high Re. For the limit $Re \to \infty$, (2) reduces to

$$\nabla^2\psi = 0 \tag{4}$$

in the assumption of irrotationality far upstream. In §3 we shall adopt the free-streamline model to obtain the solution of (4) applicable to the potential region.

3. Free-streamline solution and the separation position

As Re tends to infinity, the viscous effect will become confined to narrow regions. These narrow regions include the boundary layer developed upstream of the separation point, the shear layer between the potential and the recirculating regions, and perhaps any shear layers that exist within the recirculating region. The existence of inner layers is only conjectured because the present calculation for the Navier–Stokes equations revealed the possibility of multiple eddies inside the recirculating region. We assume at this time however that the detailed flow mechanism in that region is negligible in an asymptotic sense, a basic principle of the free-streamline theory. Thus our model comprises two regions, the potential one and the motionless one divided by the free streamline.

In this section we shall first find an inviscid solution for the potential region using classical complex-function theory, and then we shall derive an asymptotic formula representing the separation position via a reconciliation between the inviscid solution and the triple-deck requirement.

3.1. *Inviscid solution*

Levi-Civita's method (see e.g. Gurevich 1966) will be used to obtain the solution of this problem. For the complex potential $W = \phi + i\psi$ the complex velocity is

$$\frac{dW}{dZ} = V\exp(-i\theta),$$

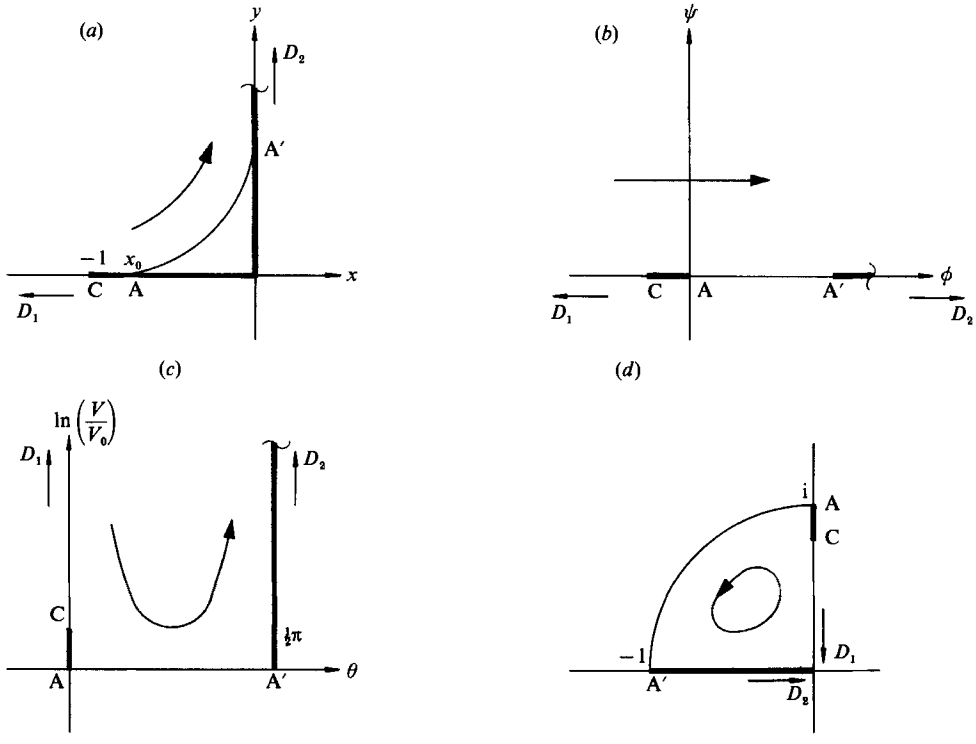

FIGURE 2. Physical and transform planes: (*a*) Z-plane, (*b*) W-plane, (*c*) ω-plane, and (*d*) ζ-plane.

where $Z = x+\mathrm{i}y$ is the complex coordinate, V is the absolute velocity, and θ is the angle that the velocity vector makes with the x-axis. In the usual manner we define ω as

$$\omega = \mathrm{i}\ln\left(\frac{1}{V_0}\frac{\mathrm{d}W}{\mathrm{d}Z}\right) = \theta + \mathrm{i}\ln\left(\frac{V}{V_0}\right), \tag{5}$$

where V_0 is the velocity on the free streamline, at present unknown. Then in the ω-plane, the boundary constitutes a semi-infinite strip (figure 2*a*, *c*). The mapping $\omega \leftrightarrow W$ is established by the Schwarz–Christoffel transformation:

$$\omega = C_1 \int \frac{\mathrm{d}W}{W^{\frac{1}{2}}(W-\phi_0)^{\frac{1}{2}}} + C_2, \tag{6}$$

where ϕ_0 is the value of W at point A′ (figure 2*b*). The upper half of the W-plane is next mapped to the interior of the quarter-circle in the ζ-plane (figure 2*d*) by

$$W = \tfrac{1}{4}\phi_0\left(\zeta - \frac{1}{\zeta}\right)^2, \tag{7}$$

upon which (6) reduces to

$$\omega = -\mathrm{i}\ln(-\mathrm{i}\zeta). \tag{8}$$

Thus from (5), (7) and (8) we obtain

$$Z = -\frac{\phi_0}{2V_0}\mathrm{i}\left(\frac{1}{3}\zeta^3 + \frac{1}{\zeta}\right). \tag{9}$$

To attain $W \to -Z^2$ for $|Z| \to \infty$ we must require

$$\phi_0 = V_0^2. \tag{10}$$

Evaluating Z at $\zeta = \mathrm{i}$ from (9) gives x_0, the x-coordinate of point A (figure 2*a*):

$$x_0 = -\tfrac{2}{3}V_0. \tag{11}$$

Note that as $x_0 \to -1$ (breakaway occurring at C, the leading edge), $V_0 \to \frac{3}{2}$.

3.2. *Asymptotic prediction for the position of the separation point*

Sychev (1972) stated in his translated article that, 'The theory of jet flows of an ideal liquid with free streamline contains all the necessary information concerning the local behaviour of the potential flow outside the region of the boundary layer close to the separation point'. Smith (1982) in his review article also showed that local shape of the free streamline satisfies the requirement of the triple-deck structure for the mass separation. In Smith's previous paper (Smith 1977), the shape of the displacement far downstream for self-consistent boundary-layer separation must be in terms of the local coordinates $(\bar{x}, \bar{y})$:

$$\bar{y} = \tfrac{2}{3}\epsilon^{\frac{1}{2}}\lambda^{\frac{9}{8}}\alpha(\bar{x}-\bar{x}_0)^{\frac{3}{2}}, \tag{12}$$

in which λ is the skin-friction coefficient to be supplied by the boundary-layer calculation for the upstream region, $\epsilon = Re_s^{-\frac{1}{8}}$ (Re_s is Reynolds number based on the local lengthscale and reference velocity), $\bar{x}_0$ denotes the $\bar{x}$-coordinate at the breakaway point, and $\alpha = 0.44$ is a constant required for the existence of the solution. We note that in (12) ϵ and λ are dependent upon the choice of the local coordinate system $(\bar{x}, \bar{y})$.

We next find the asymptotic shape of the free streamline near the breakaway point A for the present problem. We set $\zeta = \exp[\mathrm{i}(\sigma + \frac{1}{2}\pi)]$ so that as the point A is approached σ tends to zero. Then (9) expands like

$$Z = (x_0 + V_0\sigma^2 + \ldots) + \mathrm{i}(\tfrac{2}{3}V_0\sigma^3 + \ldots). \tag{13}$$

Thus for small σ the shape of the free streamline is represented to leading order by

$$y = \tfrac{2}{3}V_0^{-\frac{1}{2}}(s-s_0)^{\frac{3}{2}} \tag{14}$$

where $s = 1+x$ and $s_0 = 1+x_0$. We choose s_0 (the distance of the breakaway point from the leading edge) as the local reference length; then $\bar{x}_0 = 1$ in (12). We also choose $\frac{3}{2}$ (the value of V_0 when the breakaway occurs at the leading edge) as the local reference velocity; then $Re_s = (3/2\nu)\,s_0$ and $\lambda = 0.332$ (the skin-friction coefficient of the Blasius flow at unit distance from the leading edge) are obtained. Recalling that $Re = 1/\nu$ (the Reynolds number used in the Navier–Stokes equations), we find $Re_s = \frac{3}{2}s_0 Re$, $\epsilon = (\frac{3}{2}s_0 Re)^{-\frac{1}{8}}$. For the function (14) to be matched with (12), (s, y) must be scaled by s_0 so that $s = s_0\bar{x}$, $y = s_0\bar{y}$ upon which (14) becomes

$$\bar{y} = \tfrac{2}{3}V_0^{-\frac{1}{2}}(\bar{x}-1)^{\frac{3}{2}}s_0^{\frac{1}{2}}. \tag{15}$$

Equating (15) and (12) with ϵ represented by s_0 and Re yields

$$s_0 = (\tfrac{3}{2})^{\frac{7}{9}}\lambda^2\alpha^{\frac{16}{9}}Re^{-\frac{1}{9}} = 0.035Re^{-\frac{1}{9}}. \tag{16}$$

This formula determines the breakaway point, the corresponding free streamline for which represents the displacement far downstream that guarantees self-consistent

separation with given Re. Now $(s_s - s_0)$, the distance between the breakaway point and the separation point, is of order $Re_s^{-\frac{3}{8}}$ the triple-deck scale; in terms of Re it is

$$s_s - s_0 = O(Re^{-\frac{1}{3}}). \tag{17}$$

Thus the order of $(s_s - s_0)$ is lower than that of s_0, which means that (16) also serves to predict the separation position for $Re \to \infty$ to leading order.

However, for the range of Re used in the computation of the full Navier–Stokes equations in §4, s_0 calculated by (16) turned out to be much smaller than s_s obtained by the numerics. Thus for practical purposes we add (17) to (16):

$$s_s = 0.035 Re^{-\frac{1}{6}} + C Re^{-\frac{1}{3}} \tag{18}$$

where C is to be determined with the aid of the numerical results.

It should be mentioned here that terms between $O(Re^{-\frac{1}{6}})$ and $O(Re^{-\frac{1}{3}})$ could be inserted in (18) depending on the local flow mechanism near the separation point. We, however, have not looked into the higher-order flow mechanism, but simply found that, in fitting the numerical results of the Navier–Stokes equations, $Re^{-\frac{1}{3}}$ was far better than $Re^{-\frac{5}{16}}$ (lower than $Re^{-\frac{1}{3}}$) or $Re^{-\frac{7}{16}}$ (higher than $Re^{-\frac{1}{3}}$).

4. Numerical solution method for the Navier–Stokes equations

Basically the numerical algorithm used in the present study is same as that developed by Fornberg (1980, 1986). A precise description of the method will not be repeated here: only its properties that are peculiar to this problem will be described. The centred-difference method is employed in approximating all the derivatives in the governing equations, which guarantees the second-order accuracy. There is only one dependent variable, ψ, in the equations so that instabilities which may arise owing to introduction of the artificial time in the stream-function–vorticity system should not spoil the iteration process at high Reynolds numbers (Fornberg 1980). The nonlinear convection terms are linearized by Newton's method to assure the quadratic convergence. At the boundary between the inviscid zone and the calculation domain, a scheme of interaction (equation (23)) between the two regions is used to reduce the effect of the domain's finiteness.

To choose a coordinate system suitable for the numerics, we must take the local nature of the flow field into account. The three regions to be considered in this problem are the leading edge, the region far downstream, and the corner.

To incorporate the features of the first two regions, we introduce the conformal mapping

$$\rho^2 = 1 - Z^2, \tag{19}$$

where $\rho = \xi + i\eta$ is associated with the calculation domain. It is easy to show that the system of coordinate (ξ, η) is optimal (Kaplun 1954) for the two regions. Although an important disadvantage of this mapping is that the Jacobian tends to zero as the corner is approached, it has some advantages: the boundary conditions on the solid wall are simply represented, and the upper boundary (at $\eta = \eta_e$) follows well the equivorticity lines which result from the economic grid system. The grid system generated by the mapping (19) is shown in figure 3.

We then replace the stream function ψ by Ψ perturbed from the asymptotic $(\eta \to \infty)$ solution of Hiemenz flow and defined by

$$\psi = 2\xi(\eta - \eta_w) + \Psi, \tag{20}$$

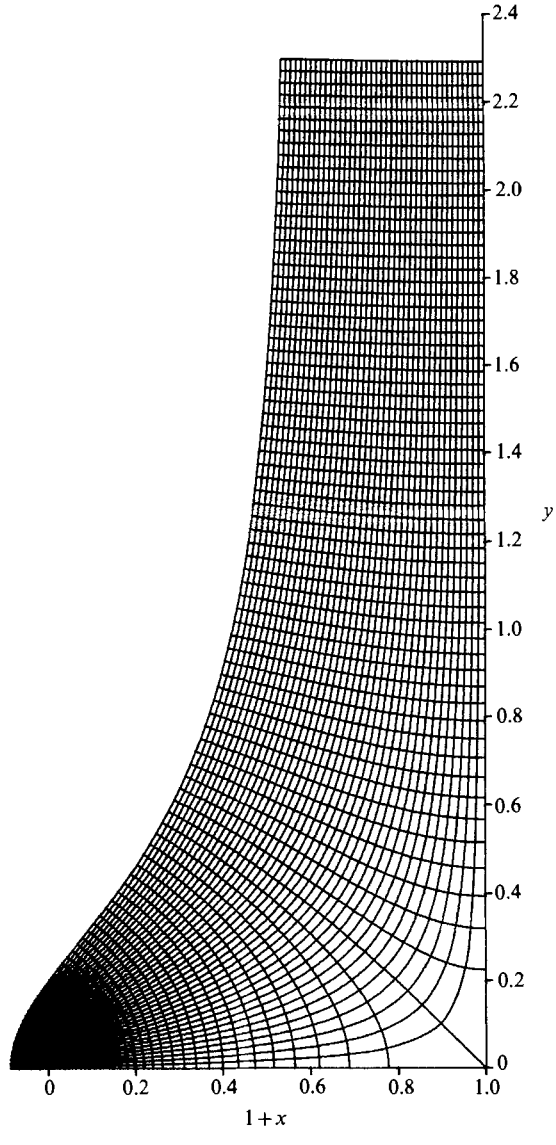

FIGURE 3. A rectangular grid in the ρ-plane shown in the Z-plane.

where $2\xi\eta_w$ represents the displacement thickness of the Hiemenz flow. Explanation for this change will be given later when the boundary conditions are considered.

With (19) and (20). the governing equation (2) is written as

$$\nabla^4\Psi+\left[\frac{2}{M}\frac{\partial M}{\partial\eta}+2Re(\eta-\eta_w)\right]\frac{\partial}{\partial\eta}\nabla^2\Psi+\left[\frac{2}{M}\frac{\partial M}{\partial\xi}-2Re\,\xi\right]\frac{\partial}{\partial\xi}\nabla^2\Psi$$
$$+\left[\frac{1}{M}\nabla^2M+\frac{2Re}{M}\frac{\partial M}{\partial\eta}(\eta-\eta_w)-\frac{2Re}{M}\frac{\partial M}{\partial\xi}\xi\right]\nabla^2\Psi$$
$$+Re\left[\frac{\partial\Psi}{\partial\xi}\frac{\partial}{\partial\eta}\nabla^2\Psi-\frac{\partial\Psi}{\partial\eta}\frac{\partial}{\partial\xi}\nabla^2\Psi+\left(\frac{1}{M}\frac{\partial M}{\partial\eta}\frac{\partial\Psi}{\partial\xi}-\frac{1}{M}\frac{\partial M}{\partial\xi}\frac{\partial\Psi}{\partial\eta}\right)\nabla^2\Psi\right]=0, \quad (21)$$

where the Jacobian M is given by $M = |\mathrm{d}\rho/\mathrm{d}Z|^2$. Formal application of Newton's method to (21) yields the following linearized equation:

$$\mathrm{A}\Psi = \mathrm{B}\bar{\Psi}, \tag{22}$$

where $\bar{\Psi}$ is a known function, and A and B are linear operators, coefficients of which are composed of M and derivatives of M and $\bar{\Psi}$. Suh (1986) contains detailed formulae for A and B.

The mathematical domain to be considered is a quarter-plane ($0 \leqslant \xi, 0 \leqslant \eta$) which is truncated at $\xi = \xi_\mathrm{m}$ and $\eta = \eta_\mathrm{m}$ for the computational domain Then we consider boundary conditions in terms of ψ or Ψ depending on convenience. Along the axis of symmetry($\xi = 0$), $\psi = \nabla^2\psi = 0$ and at the surface of the plate and wall ($\eta = 0$), $\psi = \partial\psi/\partial\eta = 0$. At the downstream edge ($\xi = \xi_\mathrm{m}$). $\partial^2\psi/\partial\xi^2 = 0$ and $(1/\xi)\,(\partial^2\psi/\partial\eta^2)$ is a function of η; these conditions are based on the boundary-layer solution for Hiemenz flow. At the top boundary ($\eta = \eta_\mathrm{m}$) one condition is $\nabla^2\psi = 0$. In choosing the other one at this boundary, care must be taken. Fornberg (1980) discussed in detail the effects of various types of conditions on the solution. The most important feature in the conditions he used in calculating steady flow over a circular cylinder (Fornberg 1986) and that over a sphere (Fornberg 1988) is that the 'infinite' nature of the actual domain can influence the finite domain of computation so that eddies in the wake may develop as freely as possible. This choice seems to be crucial in his studies since the width of the eddy for each obstacle increased by the same order as its length as Reynolds number increases, when it is high. Thus it is natural to adopt Fornberg's idea in this study since we have as yet no information on the eddy's properties. What happens in the computational domain disturbs the inviscid zone ($\eta > \eta_\mathrm{m}$) where the governing equation is $\nabla^2\Psi = 0$ with the boundary condition $\Psi = \Psi(\xi, \eta_\mathrm{m})$ at $\eta = \eta_\mathrm{m}$. Solution of this problem then gives $\Psi(\xi, \eta_\mathrm{m} + \Delta\eta)$;

$$\Psi(\xi, \eta_\mathrm{m} + \Delta\eta) = \frac{\Delta\eta}{\pi}\int_{-\infty}^{\infty} \frac{\Psi(t, \eta_\mathrm{m})}{(\xi - t)^2 + \Delta\eta^2}\,\mathrm{d}t. \tag{23}$$

This is in turn used in constructing the finite-difference formula for the grid points near $\eta = \eta_\mathrm{m}$.

To evaluate this integral we need $\Psi(\xi, \eta_\mathrm{m})$ for $\xi > \xi_\mathrm{m}$. First we note from (20) that $\Psi(\xi, \eta_\mathrm{m})$ tends to zero as $\xi \to \infty$. Consequently it will suffice to assign $\Psi(\xi, \eta_\mathrm{m}) = \Psi(\xi_\mathrm{m}, \eta_\mathrm{m})$ for $\xi > \xi_\mathrm{m}$; this explains the reason for (20).

The centred-difference method was applied to obtain the discretized equation for (22). Six unknowns are associated with resolving the right-hand side of (23); they are $\Psi(\xi - 2\Delta\xi, \eta_\mathrm{m})$, $\Psi(\xi - \Delta\xi, \eta_\mathrm{m})$, $\Psi(\xi, \eta_\mathrm{m})$, $\Psi(\xi + \Delta\xi, \eta_\mathrm{m})$, $\Psi(\xi + 2\Delta\xi, \eta_\mathrm{m})$, and $\Psi(\xi_\mathrm{m}, \eta_\mathrm{m})$. Accordingly the discretized equations for $I \times J$ grid points give a coefficient matrix similar to the block penta-diagonal as shown in figure 4 where the unknown column matrix is composed of vectors $\phi_i = (\Psi_{i,2}, \Psi_{i,3}, \ldots, \Psi_{i,J})^\mathrm{T}$ $(i = 2, 3, \ldots, I)$. Each block is of size $(I-1) \times (J-1)$ and diagonalized form. Gaussian elimination was employed to eliminate the block elements below the diagonal. During both this elimination process and the back substitution process, LU-decomposition with partial pivot was used in inverting the block element.

The sequence of computation is as follows:

(i) Initialize $\Psi_{i,j}$. (ii) Generate the coefficient matrix and the load vector. (iii) Solve the matrix for ϕ_i. (iv) Test for convergence (criterion;

$$\max\begin{bmatrix} 2 \leqslant i \leqslant I \\ 2 \leqslant j \leqslant J \end{bmatrix} |\Psi_{ij}^{\mathrm{new}} - \Psi_{ij}^{\mathrm{old}}|$$

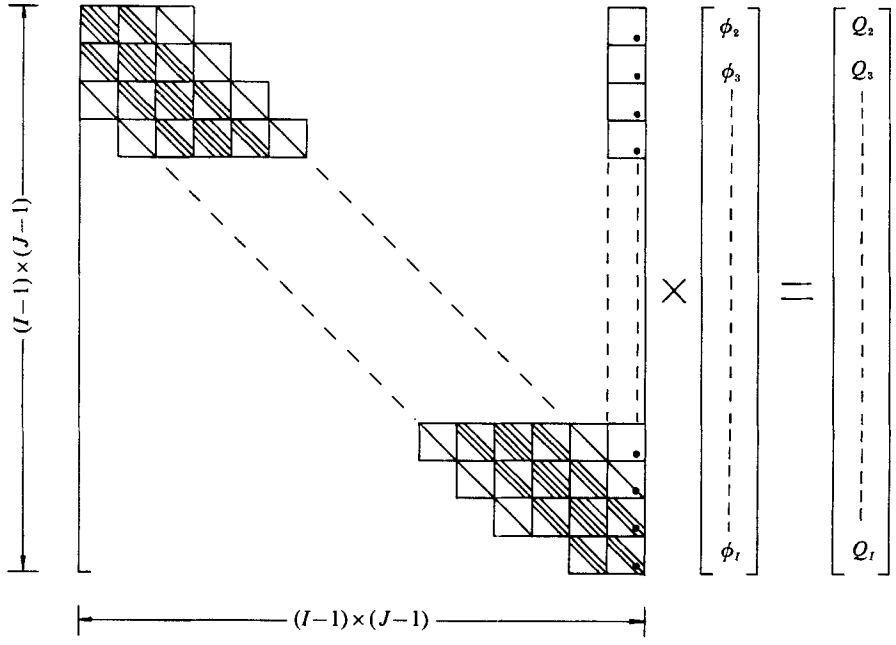

FIGURE 4. Structure of the linear system generated by applying Newton's method to the Navier–Stokes equations.

should be less than 10^{-3}). (v) Repeat (ii) to (iv) until the convergence criterion is satisfied.

5. Results and discussions

On the basis of several test runs, $\xi_m = 2.5$, $\eta_m = 6/(2 \times 100)^{\frac{1}{2}}$, $I = 101$, and $J = 41$ are selected for optimal values. Selection of η_m is on the basis that this value is just enough to contain the boundary layer of Hiemenz flow at $Re = 100$, the starting Re in the present calculation, and it is also enough to cover the recirculating region even when Re tends to infinity (based on the result of §3). Starting from 100, Re was increased carefully (the solution at each Re was used as the initial value at the next higher Re, except for $Re = 100$ at which the Hiemenz solution was utilized) in such a way that the iteration process for a given Re converges in a few cycles; the increments of Re were 100 up to $Re = 800$, 200 up to $Re = 1600$, and 400 up to $Re = 2800$. Too large an increase in Re raised the convergence problem. For instance the jump $200 \rightarrow 400$ in Re failed to give a converged solution. We also found that although up to $Re = 5000$ there was no problem in convergence or stability, for $Re \geqslant 2800$ oscillations in vorticity distributions occurred, specifically downstream of the recirculating region (figure 6*e*). Such oscillations are without doubt due to the coarse meshes for the given Re. Results at $Re = 2800$ are, however, used in the following analysis assuming that the regions of interest are still safe.

Computation was conducted in CYBER 730 with 14-digit precision. CPU time consumed for each Newton iteration was approximately 10 minutes.

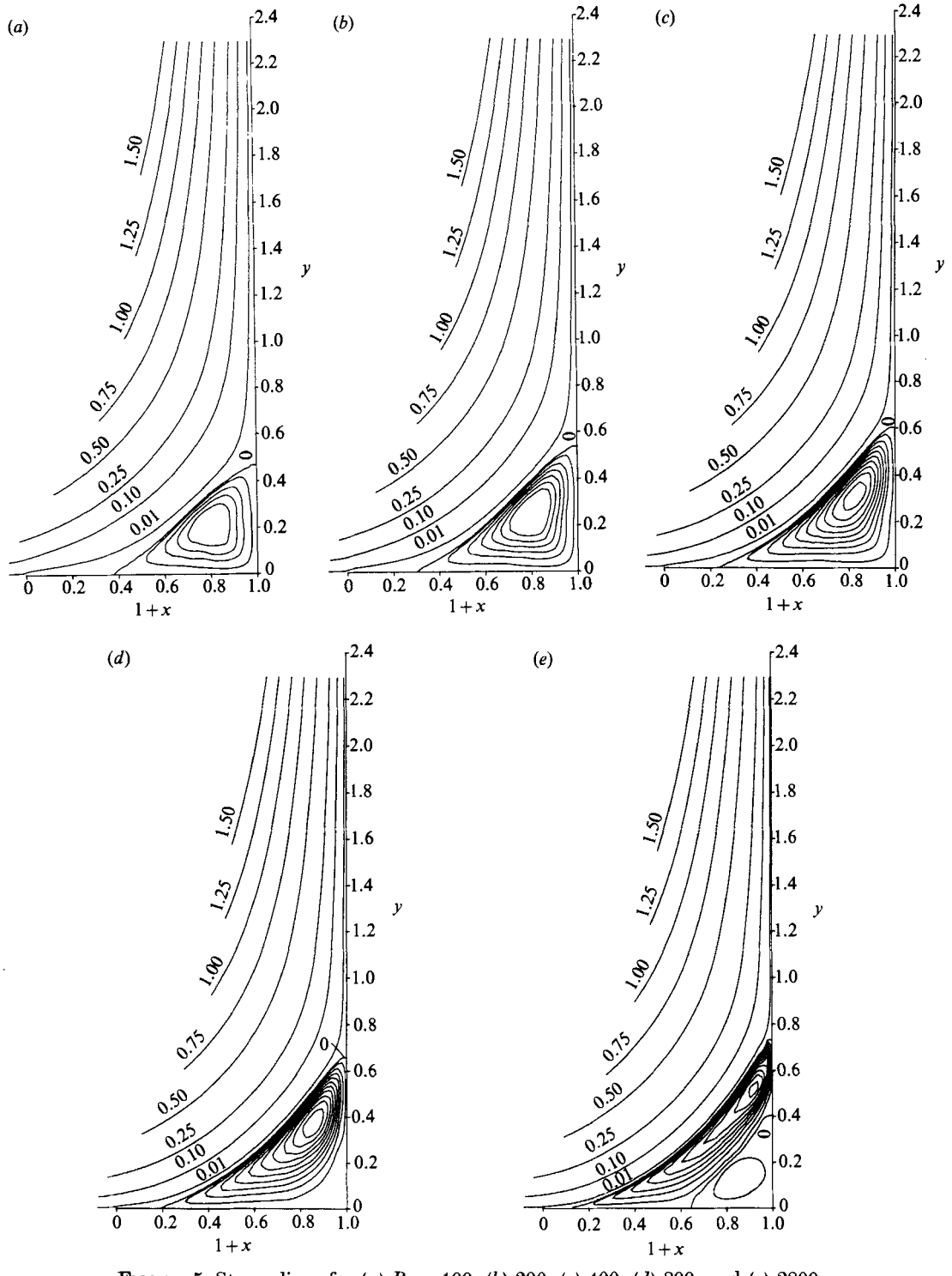

FIGURE 5. Streamlines for (*a*) $Re = 100$, (*b*) 200, (*c*) 400, (*d*) 800, and (*e*) 2800.

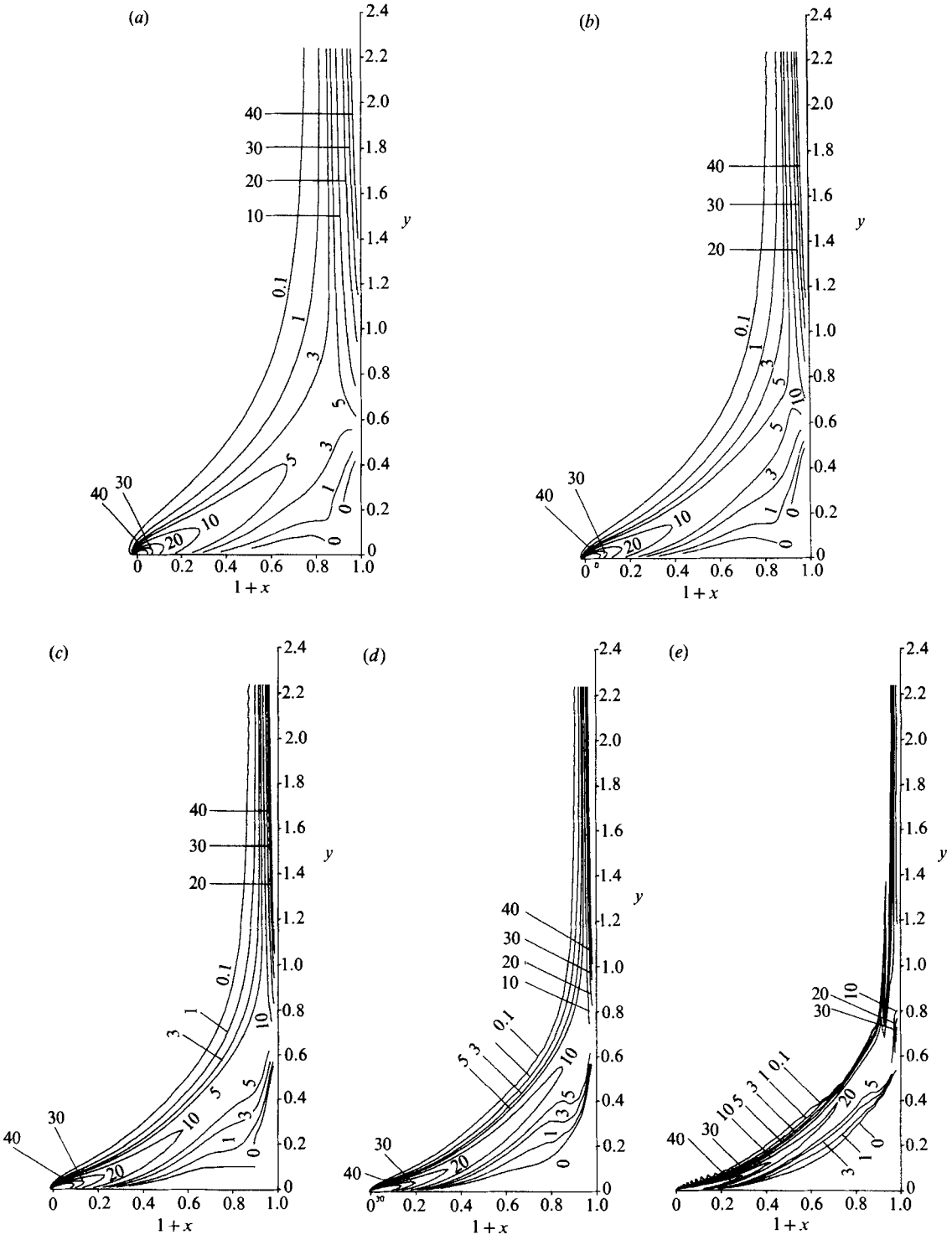

FIGURE 6. Equivorticity lines for (*a*) $Re = 100$, (*b*) 200, (*c*) 400, (*d*) 800, and (*e*) 2800.

5.1. *The structure of recirculated flow*

Figure 5 shows the streamlines and figure 6 the equivorticity lines at $Re = 100$, 200, 400, 800, and 2800. First we note that secondary eddies appear at Re higher than 800: in fact the secondary eddy began to emerge at $Re = 1000$. We can find similar features in the flow around bottom corners in the lid-driven-cavity problem (see Ghia, Ghia & Shin 1982 and Gresho *et al.* 1984). Regarding the development of eddies near the corner we draw on the discussion by Burggraf (1966). (Our discussion in the following is only tentative since the lid-driven-cavity problem and ours cannot be directly compared.) He showed that the primary ('second' in his notation) eddy that occurred in a bottom corner of the lid-driven cavity could be described by the Stokes model based on the analysis of Moffatt (1964) (Burggraf pointed out that the effective Reynolds number characteristic of the primary eddy was only about 1.6 even though the global value is 400). On the other hand, following Moffatt (1964) the corner intrinsically contains locally an infinite sequence of eddies (higher resolution of the grid system might have shown more eddies in the present calculation), and owing to the similarity nature each eddy would recede from the singular point (the corner) as the intensity of the disturbance far from the corner increases; in the present problem an increase of the disturbance intensity is associated with an increase of Re. It is obvious that in the region sufficiently close to the corner the viscous effect is dominant (owing to the low effective Reynolds numbers) so that the Stokes model is applicable. But it is also thought that the eddies that developed earlier (typically the primary eddy) are susceptible to the effectively high-Re flow since shear layers and the flow mechanisms near the reattachment points would induce sufficiently high velocity within eddies. Thus at asymptotically large Reynolds numbers the primary eddy will be primarily inviscid and the Moffatt description will only apply to the eddies very close to the corner.

Our results locally exhibit a slight indication of viscous to inviscid transition of the primary eddy; three consecutive figures (figure 6*c*, *d* and *e*) show that near the vortex centre the flow field tends to have uniform vorticity at higher Re.

On the other hand, Leal (1973) also found that at $Re = 200$, which was the highest Re used in his numerics, the primary eddy could be described more accurately by the Stokes model than by the inviscid one. It appears that $Re = 200$ is not high enough for the primary eddy to be described by the inviscid model. In order to obtain more reliable features we need to construct finer meshes in the numerics for higher-Reynolds-number flow.

5.2. *The nature of the potential flow field*

Regardless of the detailed nature of the recirculating flow, we can demonstrate an important and distinctive feature in the development of the potential flow. In the following we shall show numerically that the free-streamline model given in §3 is the right description of the potential-flow field in the limit $Re \to \infty$. Figure 7 shows streamlines obtained by the Navier–Stokes calculation compared to those of the free-streamline model in the potential region; the results of the free-streamline model correspond to the leading-edge breakaway. It is seen on the whole that as Re is increased the Navier–Stokes solutions tend to fit the free-streamline solutions. The discrepancy shown at lower Re in the downstream region is due to the effect of the boundary-layer displacement. The separating streamline (the streamline of $\psi = 0$ in the Navier–Stokes solutions) is inclined to approach the breakaway streamline (the streamline of $\psi = 0$ in the free-streamline solutions). A somewhat reversed trend in

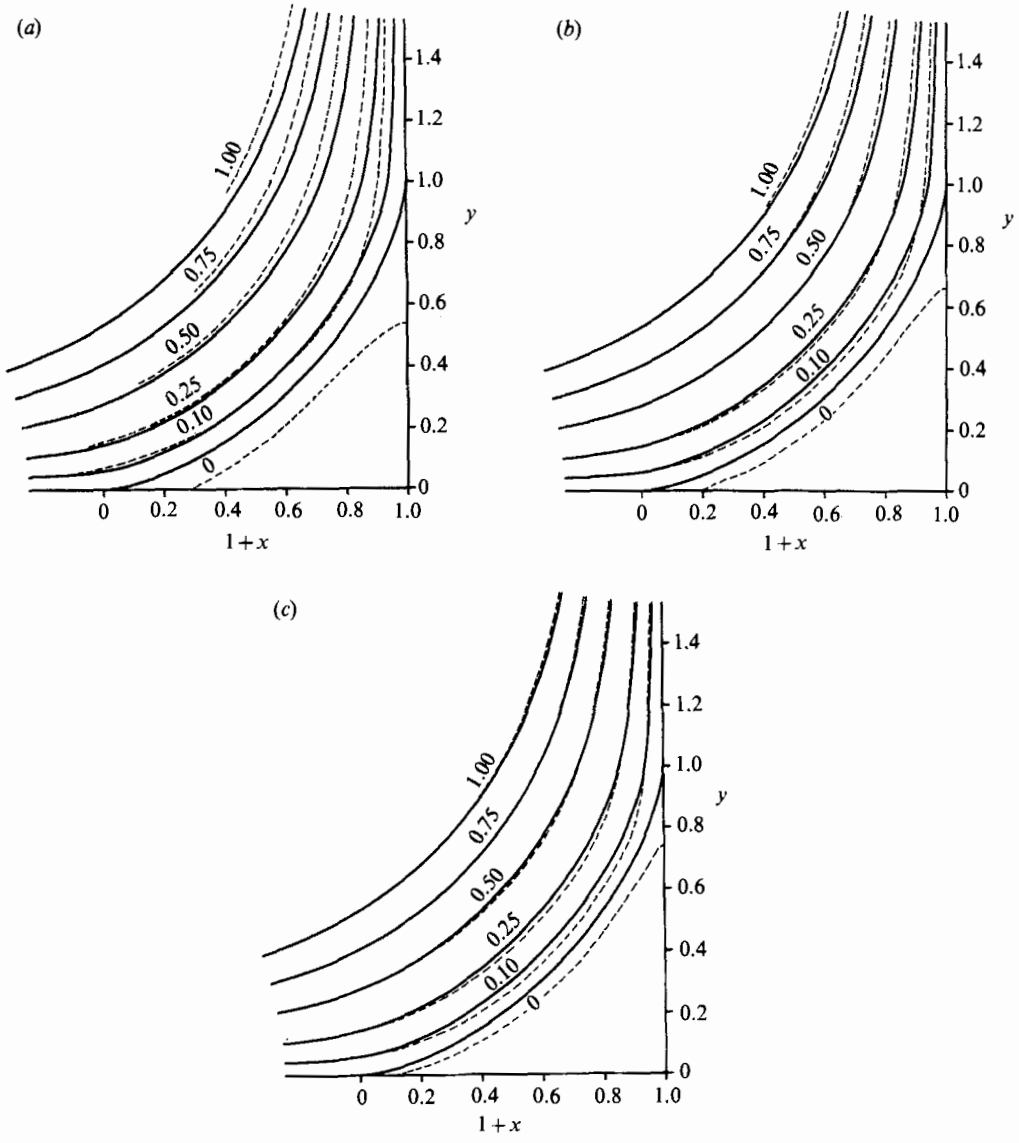

FIGURE 7. Streamlines obtained by the free-streamline model with the breakaway point at the leading edge (——); and those by the Navier–Stokes equations (– – – –) for (*a*) $Re = 200$, (*b*) 800, and (*c*) 2800.

the $\psi = 0.10$ and 0.25 streamlines in the neighbourhood of the separating streamline can be tentatively explained by the shear-layer effect as well as their location. That is, when Re is increased the separating streamline recedes from the corner pushing the streamlines of $\psi > 0$ outward, whilst the thickness of the shear layer is decreased resulting in the reverse effect, and thus if the latter effect is temporarily bigger than the former one it will lead to the result found. However, it can reasonably be conjectured that as Re is increased further the value of ψ with the discrepancy would tend to zero. In an attempt to compare shapes of the $\psi = 0$ streamlines, V_0 (see §3) is adjusted such that the free streamline best fits the separating streamline as shown in figure 8; here, $s_0 = 0.08$ and $V_0 = 1.38$. Also shown are the results of Chernyshenko

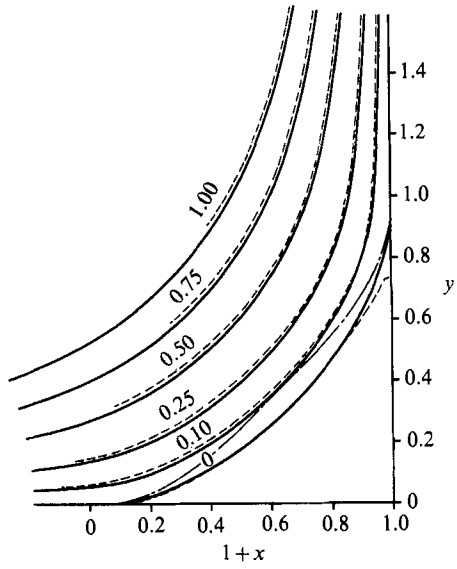

FIGURE 8. Streamlines obtained by the free-streamline model with the breakaway point $s_0 = 0.08$ (——), and those by the Navier–Stokes equations for $Re = 2800$ (– – –). Also shown is the breakaway streamline obtained by Chernyshenko (1984) based on Batchelor's single-eddy model (— — —).

(1984) via Batchelor's model (single eddy in the recirculating region). It is seen that the free streamline perfectly fits the separating streamline except for the local region near the reattachment point. On the other hand, the line predicted by the use of the single-eddy model with a specific non-zero vorticity does not seem to be fitted by the separating streamline. It also appears from figure 9 of Moore, Saffman & Tanveer (1988) that the best fit is obtained when the vorticity is zero.

It is natural at this stage to investigate how the constant pressure established along the shear layer would influence the recirculating region, including the solid surface. The surface pressure gradient is given by

$$\frac{\partial p}{\partial s} = \frac{1}{Re}\left[\frac{(1-\xi^2)^{\frac{1}{2}}}{\xi}\right]^3 \frac{\partial^3 \Psi}{\partial \eta^3}(\xi, 0), \tag{24}$$

where s is the distance of a point on the surface measured from the leading edge of the plate and $(\partial^3\Psi/\partial\eta^3)(\xi, 0)$ is evaluated with the use of three consecutive Ψ values near the surface. Distributions of $\partial p/\partial s$ are shown in figure 9. Particular features observed at high Re are that the pressure gradient tends to zero over the recirculating region, and that regions near the separation and reattachment point have a tendency to have large local positive values – a similar but less distinctive trend was also observed by Leal (1973).

The first feature mentioned above means that the pressure field in the recirculating region is dominated by that of the potential region. This forms a striking contrast to that of a circular cylinder (Fornberg 1986) or a sphere (Fornberg 1988) in a uniform stream in which the self-established inviscid flow field leads to an absolutely independent pressure field.

The large positive pressure gradient near the reattachment point on the solid surface was favoured by many investigators (Smith & Duck 1977; Smith 1979; and

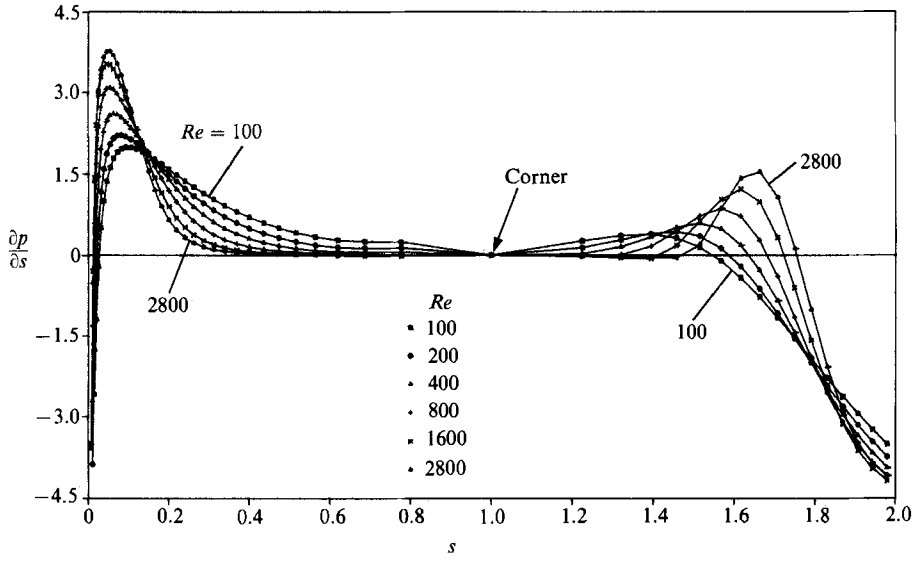

FIGURE 9. Distributions of the surface pressure gradient $\partial p/\partial s$.

Re	s_s
200	0.301
400	0.237
800	0.188
1600	0.151
2000	0.142
2800	0.130

TABLE 1. Position of the separation point s_s obtained by the numerical solution of the Navier–Stokes equations

Smith & Merkin 1982). Exact solutions of the Navier–Stokes equations for non-orthogonal stagnation-point flow presented by Tamada (1979) and Dorrepaal (1986) may describe the flow field in the neighbourhood of the reattachment point (refer to Peregrine 1981, 1985 for the symmetric boundary condition such as treated by Leal 1973). But the question remains as to how such solutions can be matched with, for instance, the potential-flow solution upstream.

The trend in the distribution of the pressure gradient near the separation point at high Re shown in figure 9 is qualitatively consistent with the requirement of the Sychev–Smith model for self-consistent boundary-layer separation.

5.3. *The position of the separation point*

Table 1 lists and figure 10 plots values of s_s obtained from the full equations of motion and those from (18) where $C = 1.631$ is given by fitting data at $Re = 2800$. A remarkable point to note is that (18) fits the numerical results to within a 0.6% relative error (at $Re = 800$) over a wide range of Re. This clearly supports the Sychev–Smith model for separation from a smooth surface. It should be mentioned however that the magnitude of the leading-order term of (18) is 6.5–11% of the total. This contradicts the asymptotic theory which is the basis of (18). This is apparently

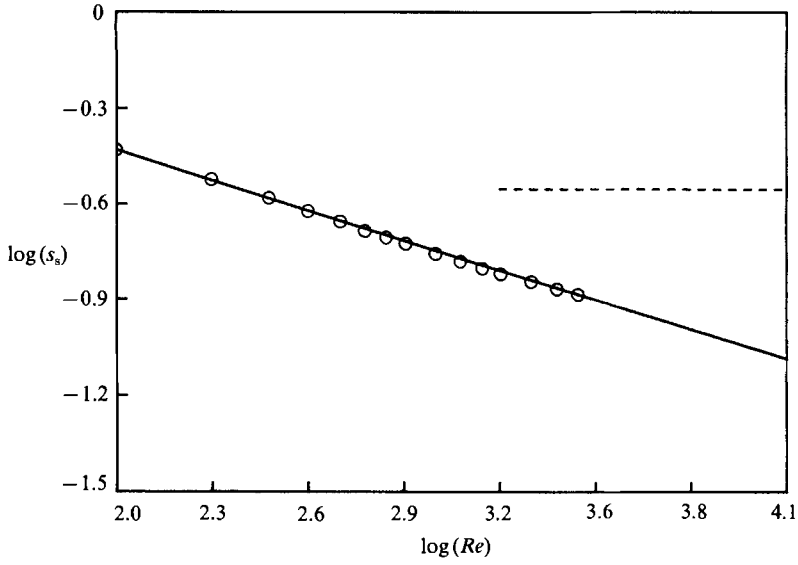

FIGURE 10. The position of the separation point: ○, numerical solution of the Navier–Stokes equations; ——, the asymptotic formula (18) with $C = 1.631$; – – – –, $s_s = 0.28$ predicted by Leal (1973).

resolved by increasing Re; however, according to (18) $Re = 3.2 \times 10^7$ is required for the first term to overtake the second one, which is far beyond the capability of presently existing computers. Another possibility may be to change the corner angle (presently 90°) so that the plate is now attached on the apex of the wedge.

On the other hand, Leal's (1973) prediction turned out not to be useful (figure 10). He obtained the limit of the separation position by applying the pressure gradient from the Navier–Stokes results at $Re = 200$ to the boundary-layer equations. The clear objection to his prediction is that the pressure gradient that he used in the boundary-layer calculation was asymptotically incorrect.

6. Conclusions

Based on the preceding text, we can draw the following conclusions.

(i) Newton's method was successfully applied to the full Navier–Stokes equations for the present problem for Re up to 2800.

(ii) The primary eddy has a slight tendency of transition from a viscous to an inviscid nature at high Re. There emerged a secondary eddy near the corner at $Re = 1000$. It was conjectured that the corner intrinsically contains an infinite sequence of eddies and that the number of inviscid eddies would increase as Re is increased.

(iii) In a global structure, there are two main regions: the recirculating region around the corner and the potential region elsewhere. It turned out that the streamlines in the potential region obtained from the full Navier–Stokes equations tend to fit those of the free-streamline model at high Re.

(iv) We found an asymptotic formula based on the Sychev–Smith model which predicted the separation position to within a 0.6% error for the range $100 \leqslant Re \leqslant 2800$. The present study thus renders further support to the Sychev–Smith model for self-consistent boundary-layer separation from a smooth surface.

The first author would like to thank the faculty in the Department of Mechanical and Aerospace Engineering, State University of New York at Buffalo for their warm considerations during his graduate study. We also thank the referees and Dr S. Cowley for useful comments and pointing out further references.

REFERENCES

BATCHELOR, G. K. 1956*a* On steady laminar flows with closed streamlines at large Reynolds number. *J. Fluid Mech.* **1**, 177–190.

BATCHELOR, G. K. 1956*b* A proposal concerning laminar wakes behind bluff bodies at large Reynolds number. *J. Fluid Mech.* **1**, 388–398.

BURGGRAF, O. R. 1966 Analytical and numerical studies of the structure of steady separated flows. *J. Fluid Mech.* **24**, 113–151.

CHERNYSHENKO, S. I. 1984 Calculation of low-viscosity flows with separation by means of Batchelor's model. *Fluid Dyn.* **19**, 206–211.

DORREPAAL, J. M. 1986 An exact solution of the Navier–Stokes equation which describes non-orthogonal stagnation-point flow in two dimensions. *J. Fluid Mech.* **163**, 141–147.

FORNBERG, B. 1980 A numerical study of steady viscous flow past a circular cylinder. *J. Fluid Mech.* **98**, 819–855.

FORNBERG, B. 1986 Steady viscous flow past a circular cylinder up to Reynolds number 600. *J. Comput. Phys.* **61**, 297–320.

FORNBERG, B. 1988 Steady viscous flow past a sphere at high Reynolds numbers. *J. Fluid Mech.* **190**, 471–489.

GHIA, U., GHIA, K. & SHIN, C. 1982 High-*Re* solutions for incompressible flow using the Navier–Stokes equations and a multi-grid method. *J. Comput. Phys.* **48**, 387–411.

GRESHO, P. M., CHAN, S. T., LEE, R. L. & UPSON, C. D. 1984 A modified finite element method solving the time-dependent, incompressible Navier–Stokes equations. Part 2; applications. *Intl J. Num. Meth. Fluids* **4**, 619–640.

GUREVICH, M. I. 1966 *The Theory of Jets in an Ideal Fluid.* Pergamon.

KAPLUN, S. 1954 The role of coordinate systems in boundary-layer theory. *Z. Angew. Math. Phys.* **5**, 111–135.

KIRCHHOFF, G. 1869 Zur Theorie freir Flüssigkeitsstrahlen. *J. Reine Angew. Math.* **70**, 289–298.

LEAL, L. G. 1973 Steady separated flow in a linearly decelerated free stream. *J. Fluid Mech.* **59**, 513–535.

MOFFATT, H. K. 1964 Viscous and resistive eddies near a sharp corner. *J. Fluid Mech.* **18**, 1–18.

MOORE, D. W., SAFFMAN, P. G. & TANVEER, S. 1988 The calculation of some Batchelor flows: the Sadovskii vortex and rotational corner flow. *Phys. Fluids* **31**, 978–990.

PEREGRINE, D. H. 1981 The fascination of fluid mechanics. *J. Fluid Mech.* **106**, 59–80.

PEREGRINE, D. H. 1985 A note on the steady high-Reynolds-number flow about a circular cylinder. *J. Fluid Mech.* **157**, 493–500.

SADOVSKII, V. S. 1971 Vortex regions in a potential stream with a jump of Bernoulli's constant at the boundary. *Appl. Math. Mech.* **35**, 729–735.

SMITH, F. T. 1977 The laminar separation of an incompressible fluid streaming past a smooth surface. *Proc. R. Soc. Lond.* A **356**, 443–463.

SMITH, F. T. 1979 The separating flow through a severely constricted symmetric tube. *J. Fluid Mech.* **90**, 725–754.

SMITH, F. T. 1982 On the high Reynolds number theory of laminar flows. *IMA J. Appl. Maths* **28**, 207–281.

SMITH, F. T. 1985 A structure for flow past a bluff body at high Reynolds number. *J. Fluid Mech.* **155**, 175–192.

SMITH, F. T. 1986 Concerning inviscid solutions for large-scale separated flows. *J. Engng Maths* **20**, 271–292.

SMITH, F. T. & DUCK, P. W. 1977 Separation of jets or thermal boundary layers from a wall. *Q. J. Mech. Appl. Maths* **30**, 143–156.

SMITH, F. T. & MERKIN, J. H. 1982 Triple-deck solutions for subsonic flow past humps, steps, concave or convex corners and wedged trailing edges. *Computers Fluids* **10**, 7–25.

SMITH, F. T. & STEWARTSON, K. 1973 Plate-injection into a separated supersonic boundary layer. *J. Fluid Mech.* **58**, 143–159.

SOUTHWELL, R. V. & VAISEY, G. 1946 Relaxation methods applied to engineering problems. XII Fluid motions characterized by 'free' stream-lines. *Phil. Trans. R. Soc. Lond.* A **240**, 15–161.

SUH, Y. K. 1986 On laminar viscous flow in a corner. Ph.D. dissertation, Department of Mechanical and Aerospace Engineering, State University of New York at Buffalo, Buffalo, New York.

SYCHEV, V. V. 1972 Laminar separation. *Fluid Dyn.* **7**, 407–417.

TAMADA, K. 1979 Two-dimensional stagnation-point flow impinging obliquely on a plane wall. *J. Phys. Soc. Japan* **46**, 310–311.

WU, TH. Y.-T. 1972 Cavity and wake flows. *Ann. Rev. Fluid Mech.* **4**, 243–284.